Available online at www.sciencedirect.com

ScienceDirect

IFAC PapersOnline CONFERENCE PAPER ARCHIVE

IFAC PapersOnLine 51-14 (2018) 294–299

Dynamics of a subthalamic nucleus-globus palidus network with three delays

B. Rahman * **Y.N. Kyrychko** ** **K.B. Blyuss** ** **S.J. Hogan** ***

* *Department of Natural Resources Engineering and Management, School of Science and Engineering, University of Kurdistan Hewler, Erbil, Kurdistan Region-F.R. Iraq (e-mail: bootan.rahman@ukh.edu.krd).*

** *Department of Mathematics, University of Sussex, Falmer, Brighton, BN1 9QH, United Kingdom (e-mail: y.kyrychko@sussex.ac.uk)*

*** *Department of Engineering Mathematics, University of Bristol Bristol, BS8 1TR, United Kingdom, (e-mail: s.j.hogan@bristol.ac.uk)*

Abstract: This paper analyses a model of the subthalamic nucleus (STN)-globus palidus (GP) network with three different transmission delays. A time-shift transformation reduces the model to a system with two time delays, for which the existence of a unique steady state is established. Conditions for stability of the steady state are derived in terms of system parameters and time delays. Numerical stability analysis is performed using traceDDE to investigate different dynamical regimes in the STN-GP model, and to obtain critical stability boundaries separating stable (healthy) and oscillatory (Parkinsonian-like) neural firing. Direct numerical simulations of the fully nonlinear system are performed to confirm analytical findings, and to illustrate different dynamical behaviours of the system.

© 2018, IFAC (International Federation of Automatic Control) Hosting by Elsevier Ltd. All rights reserved.

Keywords: Subthalamic Nucleus (STN)-Globus Palidus (GP), Time Delays, Stability Analysis.

1. INTRODUCTION

All activities, such as movement, perception and conscious experience manifest themselves in rhythmic brain oscillations, and disruption or increased activity of neural networks can lead to various brain pathologies. Neurodegenerative diseases, including Alzheimer's disease, epilepsy, Parkinson's disease, selectively disrupt these networks, affecting various neuronal functions (Götz et al., 2009). For instance, in Alzheimer's disease, the most prevalent form of dementia, a number of studies have shown a significantly reduced clustering coefficient associated with a lower local network connectivity (Supekar et al., 2008; Sanz-Arigita et al., 2010).

Parkinson's disease (PD), first identified as shaking palsy nearly 200 years ago by James Parkinson, is the second most common form of dementia. Symptoms include resting tremor, rigidity, slowness/absence of voluntary movement, and postural instability (Dauer and Przedborski, 2003). This is linked to the principal loss of dopaminergic neurons of the substantia nigra, and leads to the reduction in the level of dopamine, which plays an important role in motor control. This affects motor functions that are regulated through the network formed by the substantia nigra and other brain functions, such as striatum, globus pallidus (GP) and subthalamic nucleus (STN), which collectively form the basal ganglia (BG). The basal ganglia regulates movement, such that, without its help, the cortex is unable to coordinate a well-executed voluntary movement. Animal and human recordings have revealed the presence of neuronal beta oscillations (10-35 Hz) in the BG network that could relate to its role in motor regulation (Gatev et al., 2006). In PD, this network becomes aberrant (Smith et al., 2011; Yao et al., 2014; Zhang et al., 2014), and shows a persistent pattern of beta oscillations, especially in the STN and GP (Little and Brown, 2014).

Holgado et al. (2010) have introduced a mathematical model that explains the generation of beta oscillations in the STN-GP circuit under the assumption of the strong connection between STN and GP. Their model also takes into account a short synaptic delay between these structures in the case when the excitatory input from the cortex to STN is stronger than the inhibitory input from striatum to GP, and the synaptic time delay between the STN and GP is negligibly small. Experimental data from an animal study suggests that the delay between STN and GP is about 6 [ms] (Fujimoto and Kita, 1993; Kita et al., 2005). Pavlides et al. (2012) modified the model first introduced in Holgado et al. (2010) in order to incorporate a physiologically relevant time delay in the STN-GP interactions, and obtained improved analytic stability conditions for realistic values of the transmission delay between STN and GP neural populations.

In this paper, we analyse the stability of the system based on the original STN-GP model introduced by Holgado et al. (2010). The stability analysis performed in Holgado et al. (2010) and its later modifications made the following simplifications: the membrane time constants are exactly the same; the transmission delays in the neural populations are taken to be equal; nonlinear activation functions are replaced by linear functions. In this paper, the membrane time constants are taken to be different. Moreover, the

2405-8963 © 2018, IFAC (International Federation of Automatic Control) Hosting by Elsevier Ltd. All rights reserved.
Peer review under responsibility of International Federation of Automatic Control.
10.1016/j.ifacol.2018.07.239

three time delays in the connections between the excitatory and inhibitory populations of neurons are taken to be different. Finally, we consider a general nonlinear class of activation functions. The activation functions are not necessarily just logistic curves, since the neural population might have more than a single inflexion point (Wilson and Cowan, 1972). In Section 2, we introduce the model describing STN and GP neural populations. In Section 3, a time-shift transformation is used to reduce the number of time delays. In Sections 4 we derive analytical conditions for local stability of the steady state in the case of a non-zero delay in the self-interaction of the GP population, and an instantaneous cross-interaction between GP and STN neural populations, and give analytical conditions for local stability of the steady state in the case when there is a delay in the cross-interaction between GP and STN populations, and an instantaneous self-interaction in the GP population. Furthermore, we consider a general case and perform a stability analysis of the system in the presence of delayed self-interaction in the GP population and delayed cross-interaction between STN and GP populations. The paper concludes with a summary in Section 4.

2. MODEL

Following Holgado et al. (2010), the mean firing rate model describing the temporal evolution of the firing rates of the excitatory population of neurons, STN, denoted by $S(t)$, and the inhibitory population of neurons, GP, denoted by $G(t)$, has the form

$$\begin{aligned}\tau_S S'(t) &= F_S(-w_{GS}G(t-T_{GS}) + w_{CS}Ctx) - S(t),\\ \tau_G G'(t) &= F_G(w_{SG}S(t-T_{SG}) - w_{GG}G(t-T_{GG})\\ &\quad -w_{XG}Str) - G(t),\end{aligned} \tag{1}$$

where $T_{GS} \geq 0$, $T_{SG} \geq 0$ and $T_{GG} \geq 0$ are the transmission time delays. In particular, T_{GS} is the transmission delay from GP to STN population, T_{SG} is the transmission delay from STN to GP population, and T_{GG} is an internal self-inhibition delay in the GP population. The constants τ_S and τ_G are the time membrane constants of neurons in STN and GP populations, while Ctx and Str represent a constant level of cortical and striatal excitation of the STN and GP populations, respectively. This system of equations represents a pair of reciprocally connected STN-GP sub-populations corresponding to one of many hypothesised basal ganglia information channels (Merrison-Hort et al., 2013). The synaptic weights w_{GS}, w_{CS}, w_{SG}, w_{GG}, and w_{XG} are all non-negative constants, and represent the strength of synaptic connectivity within and between the populations, where w_{xy} is the strength of the connection from population x to population y (e.g., w_{SG} is the synaptic connectivity from STN to GP). The functions F_S and F_G are the activation functions of the STN and GP neural populations, which describe their firing rate as a function of synaptic input, and they are given by

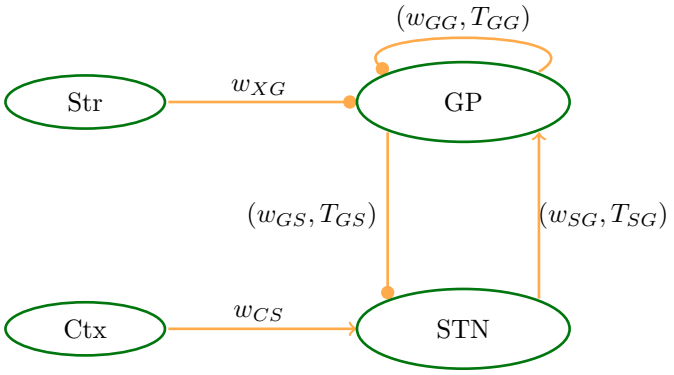

Fig. 1. Diagrammatic sketch of the STN-GP model represented by the system (1).

$$\begin{aligned}F_S(\cdot) &= \frac{M_S}{1+\left(\frac{M_S-B_S}{B_S}\right)e^{\frac{-4(\cdot)}{M_S}}},\\ F_G(\cdot) &= \frac{M_G}{1+\left(\frac{M_G-B_G}{B_G}\right)e^{\frac{-4(\cdot)}{M_G}}},\end{aligned} \tag{2}$$

where M_S and M_G are the maximum firing rates of STN and GP populations, and B_S and B_G are the STN and GP firing rates in the absence of input. A schematic diagram of the model (1) representing the dynamics of STN-GP interactions is shown in Figure 1.

The parameter values are summarised in Table 1 and are available in the literature (for details, see Holgado et al. (2010)). However, the synaptic weights were not available in the literature and, therefore, Holgado et al. (2010) found the values for which the model reproduced a wide range of experimental findings.

Table 1. Parameters and their values

Parameter	Value	Source
T_{SG}	6 ms	Kita et al. (2005)
T_{GS}	6 ms	Fujimoto and Kita (1993)
T_{GG}	4 ms	Holgado et al. (2010)
τ_S	6 ms	Kita et al. (1983), Nakanishi et al. (1987)
τ_G	14 ms	Kita and Kitai (1991)
C_{tx}	27 spk/s	Lebedev and Wise (2000)
S_{tr}	2 spk/s	Schultz and Romo (1988)
M_S	300 spk/s	Hallworth et al. (2003)
B_S	17 spk/s	Hallworth et al. (2003)
M_G	400 spk/s	Kita et al. (2005), Kita (2007)
B_G	75 spk/s	Kita et al. (2004), Kita (2007)

3. STABILITY ANALYSIS

Before starting the stability analysis of the model (1), we can reduce the number of transmission delays by using a time-shift transformation in the firing rate $S(t)$ of the STN population. In order to do this, let us introduce a new variable $\tilde{S}(t)$ as follows

$$\tilde{S}(t) = S(t+T_{GS}), \tag{3}$$

and the system (1) results in the following equivalent system

$$\begin{aligned}\tau_S\tilde{S}'(t) &= F_S(-w_{GS}G(t)+w_{CS}Ctx)-\tilde{S}(t),\\ \tau_G G'(t) &= F_G(w_{SG}\tilde{S}(t-T_1)-w_{GG}G(t-T_2)\\ &\quad -w_{XG}Str)-G(t),\end{aligned} \tag{4}$$

where $T_1 = T_{GS}+T_{SG}$, $T_2 = T_{GG}$, and the new state variable $\tilde{S}(t)$ is time-shifted relative to the original state variable $S(t)$. It is clear that both systems (1) and (4) possess the same steady states and characteristic equations. From now on, all our analysis will be based on the model (4).

3.1 Stability analysis

The system (4) possesses a non-trivial steady state $E^* = (\tilde{S}^*, G^*)$, where $\tilde{S}^*$, G^* are given implicitly by the solutions of

$$\begin{aligned}\tilde{S}^* &= F_S(-w_{GS}G^*+w_{CS}Ctx),\\ G^* &= F_G(w_{SG}\tilde{S}^*-w_{GG}G^*-w_{XG}Str).\end{aligned} \tag{5}$$

The system linearized about $E^* = (\tilde{S}^*, G^*)$ takes the form

$$\mathbf{X}'(t) = L_0\mathbf{X}(t)+L_1\mathbf{X}(t-T_1)+L_2\mathbf{X}(t-T_2), \tag{6}$$

where $L_0\, L_1$ and L_2 are given by

$$L_0 = \begin{pmatrix} -\frac{1}{\tau_S} & -\frac{r_1 w_{GS}}{\tau_S} \\ 0 & -\frac{1}{\tau_G}\end{pmatrix}, L_1 = \begin{pmatrix} 0 & 0 \\ \frac{r_2 w_{SG}}{\tau_G} & 0\end{pmatrix}, L_2 = \begin{pmatrix} 0 & 0 \\ 0 & -\frac{r_2 w_{GG}}{\tau_G}\end{pmatrix},$$

where $r_1 = \frac{4\tilde{S}^*(M_S-\tilde{S}^*)}{M_S^2}$ and $r_2 = \frac{4G^*(M_G-G^*)}{M_G^2}$. The associated characteristic matrix is

$$\Psi(\lambda, T_1, T_2) = \lambda I - L_0 - L_1 e^{-\lambda T_1} - L_2 e^{-\lambda T_2},$$

where I is the 2×2 identity matrix, and the corresponding characteristic equation becomes

$$\det[\Psi(\lambda, T_1, T_2)] \equiv \lambda^2+p_1\lambda+p_2+re^{-\lambda T_1}+(q_1\lambda+q_2)e^{-\lambda T_2} = 0, \tag{7}$$

where

$$\begin{aligned} p_1 &= \frac{\tau_S+\tau_G}{\tau_S\tau_G}, \quad p_2 = \frac{1}{\tau_S\tau_G}, \quad r = \frac{r_1 r_2 w_{GS} w_{SG}}{\tau_S\tau_G},\\ q_1 &= \frac{r_2 w_{GG}}{\tau_G}, \quad \text{and} \quad q_2 = \frac{r_2 w_{GG}}{\tau_S\tau_G}.\end{aligned} \tag{8}$$

Note that p_i, q_i, $r_i, r > 0$ for $i = 1, 2$. The transcendental equation (7) determines the stability of the steady state E^*. We consider three different cases. First, we assume that $T_1 = 0$ and $T_2 > 0$, and find stability conditions for E^*. Second, we take $T_2 = 0$ and $T_1 > 0$, and determine stability boundaries for E^* depending on the value of T_1. Finally, we analyse the stability properties of E^* in the general case when both time delays are present, $T_1 > 0$ and $T_2 > 0$.

3.2 Stability analysis: single time delay

In this section we consider the case when there is a delayed self-interaction in the GP population (i.e. $T_2 > 0$) and an instantaneous cross-interaction between STN and GP populations (i.e. $T_1 = 0$). The characteristic equation (7) reduces to

$$\lambda^2+p_1\lambda+p_2+r+(q_1\lambda+q_2)e^{-\lambda T_2} = 0, \tag{9}$$

where p_i, q_i, $i = 1, 2$, and r are given by (8). In order to determine stability boundaries, we need to determine parameter values for which $\Re(\lambda) = 0$. This can happen in two ways: $\lambda = 0$ or $\lambda = i\xi$. Clearly, $\lambda = 0$ is not a root of the equation (9). So we look for solutions of (9) in the form $\lambda = i\xi\ (\xi > 0)$, giving

$$-\xi^2+p_1\xi i+p_2+r+(q_1\xi i+q_2)(\cos\xi T_2-i\sin\xi T_2) = 0. \tag{10}$$

Separating the real and imaginary parts of (10) we get

$$\begin{cases}\xi^2-p_2-r &= q_2\cos(\xi T_2)+q_1\xi\sin(\xi T_2)\\ p_1\xi &= q_2\sin(\xi T_2)-q_1\xi\cos(\xi T_2)\end{cases} \tag{11}$$

Squaring and adding the resulting equations gives

$$\xi^4-(q_1^2+2p_2+2r-p_1^2)\xi^2+(p_2+r)^2-q_2^2 = 0. \tag{12}$$

The four roots of the equation (12) can be expressed as follows

$$\xi_\pm^2 = \frac{(q_1^2+2p_2+2r-p_1^2)\pm\sqrt{\Delta_1}}{2}, \tag{13}$$

where $\Delta_1 = (q_1^2+2p_2+2r-p_1^2)^2-4((p_2+r)^2-q_2^2)$. Depending on the values of p_i, q_i, $i = 1, 2$, and r, equation (12) can have no, one or two positive roots.

If (H1) $(p_2+r)^2-q_2^2 > 0$ and $q_1^2+2p_2+2r-p_1^2 < 0$ or $\Delta_1 < 0$, then equation (12) has no positive roots.

If (H2) $(p_2+r)^2-q_2^2 < 0$ or $q_1^2+2p_2+2r-p_1^2 > 0$ and $\Delta_1 = 0$, then the equation (12) has one positive root ξ_+.

If (H3) $(p_2+r)^2-q_2^2 > 0$, $q_1^2+2p_2+2r-p_1^2 > 0$ and $\Delta_1 > 0$, then the equation (12) has two positive roots $\xi_\pm = \frac{\sqrt{2}}{2}[q_1^2+2p_2+2r-p_1^2\pm\sqrt{\Delta_1}]^{\frac{1}{2}}$.

If either of the hypotheses (H2) or (H3) holds, the characteristic equation (9) has purely imaginary roots when T_2 takes certain values. These critical values $T_2 = T_{2\pm}^j$ can be found as follows. We can find $\sin(\xi T_2)$ and $\cos(\xi T_2)$ from a pair of equation (11) as

$$\begin{aligned}\sin(\xi T_2) &= \frac{\xi(q_1\xi^2+p_1q_2-p_2q_1-q_1r)}{q_1^2\xi^2+q_2^2},\\ \cos(\xi T_2) &= -\frac{p_1q_1\xi^2-q_2\xi^2+p2q_2+q_2r}{q_1^2\xi^2+q_2^2}.\end{aligned} \tag{14}$$

Dividing $\sin(\xi T_2)$ by $\cos(\xi T_2)$, the critical time delays can be expressed as

$$T_{2\pm}^j = \frac{1}{\xi_\pm}\left\{\tan^{-1}\left(-\frac{\xi_\pm(q_1\xi_\pm^2+p_1q_2-p_2q_1-q_1r)}{p_1q_1\xi_\pm^2-q_2\xi_\pm^2+p2q_2+q_2r}\right)+j\pi\right\}, \tag{15}$$

where $j = 0, 1, \cdots$.

In hypotheses (H2), the characteristic equation (9) has two imaginary solutions $\xi_\pm$ with $\xi_+ > \xi_- > 0$ defined in (13). In order to determine stability as T_2 varies, we need to find the sign of the derivative of $\mathrm{Re}(\lambda)$ at the points where $\lambda(T_2)$ is purely imaginary.

Lemma 1. The following transversality conditions are satisfied

$$\left[\frac{d\mathrm{Re}\{\lambda(T_2)\}}{dT_2}\right]_{T_2=T_{2+}^0} > 0, \quad \left[\frac{d\mathrm{Re}\{\lambda(T_2)\}}{dT_2}\right]_{T_2=T_{2-}^0} < 0.$$

It is worth noting that when $T_1 = T_2 = 0$, the system (4) becomes a system of ODEs with characteristic equation

$$\lambda^2+(p_1+q_1)\lambda+p_2+q_2+r = 0. \tag{16}$$

Whenever (H4) $p_1+q_1 > 0$ and $p_2+q_2+r > 0$, both roots of equation (16) with $T_1 = T_2 = 0$ always have negative real parts, and the steady state E^* is stable.

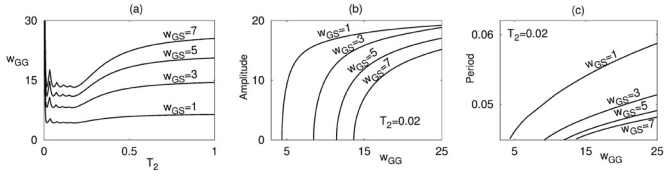

Fig. 2. (a) Stability of the non-trivial steady state E^* of the system (4) in the parameter space of the time delay T_2 and the synaptic weight w_{GG} for different values of the synaptic weight w_{GS}. The non-trivial steady state E^* is stable below the stability boundaries. (b) Amplitude and (c) period of the periodic solutions for different values of w_{GS} and $T_2 = 0.02$.

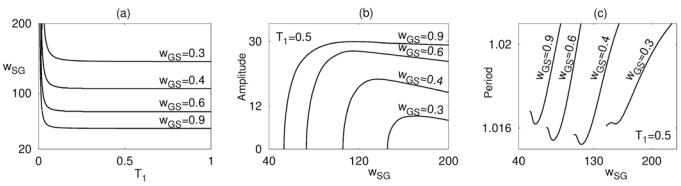

Fig. 3. Stability of the non-trivial steady state E^* of the system (4) in the parameter space of time delay T_1 and the synaptic weight w_{SG} for different values of the synaptic weight w_{GS}. The non-trivial steady state E^* is stable below the stability boundaries. (b) Amplitude and (c) period of the periodic solutions for different values of w_{GS} and $T_1 = 0.5$.

By Lemma 1 and results in Cooke and Grossman (1982), we have the following theorem,

Lemma 2. For system (4) where $T_1 = 0$ and $T_2 > 0$, suppose that (H4) holds and $T^j_{2\pm}$ are defined by equation (15), then we have

(i) If condition (H1) holds, then the steady state solution E^* of system (4) is asymptotically stable when $T_2 \geq 0$.
(ii) If condition (H2) holds, then there is a positive integer k such that there are k switches from stability to instability to stability, when $T_2 \in \bigcup_{j=0}^{k}(T^{j-1}_{2^-}, T^j_{2^+})$, where $T^{-1}_{2^-} = 0$ then the steady state solution E^* of system (4) is asymptotically stable, and when $T_2 \in \bigcup_{j=0}^{k-1}(T^j_{2^+}, T^j_{2^-})$ and $T_2 > T^k_{2^+}$, then the steady state solution E^* of system (4) is unstable.
(iii) If condition (H3) holds, then the steady state solution E^* of system (4) is stable when $T_2 \in [0, T^0_{2^+})$, undergoes a Hopf bifurcation when $T_2 = T^0_{2^+}$, and is unstable when $T_2 > T^0_{2^+}$.

In order to gain a better understanding of the stability properties of the non-trivial steady state $E^* = (\tilde{S}^*, G^*)$ given by (5) for the system (4), we use a traceDDE, a toolbox in MATLAB for computing the characteristic roots and stability charts for linear autonomous systems of delay differential equations with discrete and distributed time delays (Breda et al., 2006; Loiseau et al., 2009) to numerically calculate the stability boundaries for different values of the synaptic weights w_{GG}, w_{GS} and the time delay T_2. Figure 2(a) shows the stability boundary of the non-trivial steady state E^* for different values of the synaptic weight w_{GS}. The steady state is stable below the curves and unstable above them. As the value of the time delay T_2, which corresponds to the delayed self-interactions within the GP population, is increased, the steady state E^* undergoes a series of stability switches for certain fixed values od w_{GG}, and for large values of the time delay T_2, the stability boundary becomes almost a constant independent of T_2. Increasing the synaptic weight w_{GS} does not change the shape of the stability boundary, however, for higher values of w_{GS}, the region where the steady state E^* is stable, increases. This suggests that the region of non-oscillatory behaviour, which corresponds to the healthy functioning of the STN-GP neural populations, is larger for higher values of the synaptic connection between GP and STN populations. When the steady state E^* becomes unstable, it undergoes a Hopf bifurcation, which gives rise to stable periodic oscillations. Using DDE-BIFTOOL packages in MATLAB, in Figures 2(b) and (c), we have plotted the amplitude and period of these periodic solutions for a fixed value of the time delay T_2 and several values of the synaptic weight w_{GS}. One can see that as the values of the synaptic weight w_{GS} are increased, this results in periodic oscillations with lower amplitude and a significantly lower period.

In the case of a delayed cross-interaction between GP and STN neural populations, i.e. $T_1 > 0$, and an instantaneous self-interaction, i.e. $T_2 = 0$, the calculations are similar to the above-considered case, and the details are omitted here.

Figure 3(a) shows the stability region of steady state E^* in the (T_1, w_{SG}) plane, which is stable below the stability curves. The stability region increases for decreasing strength of the synaptic connection w_{GS} between GP and STN populations, but, unlike the case of $T_2 \neq 0$, there is just one stability switch from a stable to an unstable region with increasing T_1. Moreover, whilst the stability boundary for very small values of the time delay T_1 strongly depends on w_{SG}, it becomes constant for larger values of T_1. Biologically, the region, where the steady state E^* is stable, corresponds to the healthy functioning of the GP-STN populations, and Figure 3 suggests that a stronger connection between GP and STN networks leads to a larger region of the neural oscillations. In Figures 3(b) and (c) we fix the value of the time delay T_1, and calculate amplitude and period of the periodic solutions, which arise after the steady state becomes unstable via a Hopf bifurcation. Figure 3(b) shows that the amplitude of the oscillating solutions is increasing for small values of the synaptic weight w_{SG} between STN and GP populations and starts to drop slightly for very large w_{SG}, whereas higher values of the synaptic weight w_{GS} lead to a much higher amplitude of oscillations. The period of oscillations is shorter for small values of the synaptic weight w_{SG} and higher values of the synaptic weight w_{GS}, as illustrated in Figure 3(c).

3.3 Stability analysis: two time delays

When $T_1 > 0$ and $T_2 > 0$, the characteristic equation (7) contains two transmission delays simultaneously present, which significantly complicates analytical calculations of the stability boundaries. Thus, one should solve characteristic equation (7) numerically in order to better understand what is actually happening inside the corresponding

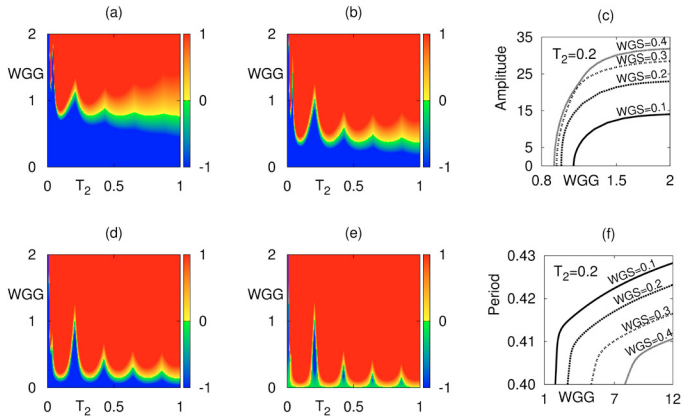

Fig. 4. Real part of the leading eigenvalue of the characteristic equation (7) with $T_1 = 0.09$, $w_{SG} = 19$, and (a) $w_{GS} = 0.1$, (b) $w_{GS} = 0.2$, (c) $w_{GS} = 0.3$ and (d) $w_{GS} = 0.4$. The colour denotes $\max[Re(\lambda)]$. (c) Amplitude of the periodic solutions for different values of w_{GS} and $T_2 = 0.2$. (f) Period of the periodic solutions for different values of w_{GS} and $T_2 = 0.2$.

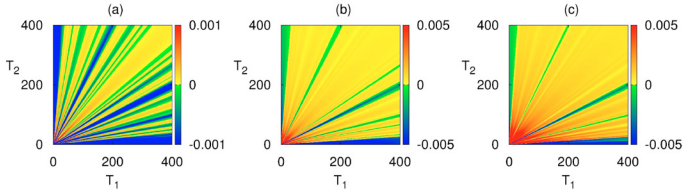

Fig. 5. Real part of the leading eigenvalue of the characteristic equation (7) for $w_{GS} = 1$, $w_{SG} = 3$ and (a) $w_{GG} = 1.6$, (b) $w_{GG} = 2$ and (c) $w_{GG} = 2.4$. Colour code denotes $\max[Re(\lambda)]$.

stability regions. In this case, it is possible to obtain an implicit expression for the stability boundary of a healthy state in (T_2, w_{GG}) plane. Substituting $\lambda = i\xi$ $(\xi > 0)$ into the characteristic equation (7) and separating real and imaginary parts, we obtain

$$\begin{cases} \xi^2 - p_2 - r\cos(\xi T_1) &= q_2\cos(\xi T_2) + q_1\xi\sin(\xi T_2), \\ p_1\xi - r\sin(\xi T_1) &= q_2\sin(\xi T_2) - q_1\xi\cos(\xi T_2). \end{cases} \tag{17}$$

Figures 4(a), (b), (d) and (e) show numerically computed maximum real part of the leading eigenvalues of the characteristic equation (17) in the (T_2, w_{GG}) plane for a fixed value of the synaptic weight w_{SG} and different values of the synaptic weight w_{GS}. From these figures, one can see that there is a finite number of stability switches between stable and unstable regimes for the same values of w_{GG}, but increasing the strength of the synaptic connection w_{GS} between GP and STN populations significantly shrinks the stability region. Figures 4(c) and (f) illustrate the amplitude and the period of the periodic solutions after the stability is lost for a fixed value of the time delay T_2. The amplitude of oscillations grows for larger values of the synaptic weights w_{GG} and w_{GS}, whilst the period of oscillations becomes smaller for larger values of w_{GS} and grows with w_{GG}.

To better understand the stability changes in the presence of two time delays, we fixed w_{GS}, w_{SG}, varied the strength w_{GG} of the self-inhibitory connection of the GP population, and numerically computed the maximum real part of the leading eigenvalue of the characteristic equation (17) in the (T_1, T_2) plane, as shown in Figure 5(a)-(c). As the value of the self-inhibitory synaptic connection w_{GG} is increased, the number of open-ended curves (stable region) decreases. This means that in the presence of two time delays and high enough values of the synaptic weight w_{GG}, the model shows oscillatory behaviour for a wide range of T_1 and T_2 values.

4. DISCUSSION

In this paper, we have studied a general subthalamic nucleus (STN) and globus pallidus (GP) network with three distinct synaptic transmission delays. Using the time-shift transformation, we reduced the original system to an equivalent system with two time delays and showed the existence of a unique non-trivial steady state. The analysis in this paper has concentrated on the stability properties of this steady state, since it has a profound effect on the dynamics of the neural populations. Biologically, the stable steady state corresponds to the healthy firing of the STN and GP populations, and if it is unstable, this results in periodic firing, which implies a Parkinsonian-type regime. To better understand the effects of different time delays on the overall stability of the system, we have divided the analysis into three different cases: delayed self-interaction in the GP population only; delayed cross-interaction between GP and STN populations only; both interactions with time delays.

For the first two cases, we have analytically found the stability regions and have shown that the non-trivial steady state is stable below some critical value of the time delay, unstable when the time delay exceeds this critical value, and undergoes a Hopf bifurcation when the time delay is equal to the critical value. Furthermore, we have numerically computed eigenvalues of the corresponding characteristic equations for the three cases, showing that the strength of the synaptic connection from the GP to STN population w_{GS} plays an important role in determining the stability of the steady state. In fact, when the time delay is only present in the self-interaction of the GP population, the stability region (healthy firing of neurons) increases with increasing w_{GS}, however, in the case when the time delay is only considered between STN and GP populations, the stability region gets larger for decreasing values of the synaptic weight w_{GS}. Moreover, the highest amplitude of oscillations in the case of the time delay being included in the self-interaction of the GP population corresponds to the lowest value of the synaptic strength w_{GS}, whilst if the time delay is only included into the interactions between STN and GP populations, the same effect on the amplitude of oscillations is observed for highest values of w_{GS}. In the case when both time delays are taken into account, the stability region shrinks if the synaptic weight w_{GS} is increased, leading to the smaller range of parameter values, where the healthy firing rate of neurons is possible, and the amplitude of oscillating solutions outside the stability region also grows for larger values synaptic weight w_{GS}.

Comparing the analysis done in this paper to the previous work in Holgado et al. (2010), it is worth noting that we

have considered the case when the activation functions are nonlinear, which gives a continuous derivative for the activation function, and rather than using the Taylor expansion under the assumption of the small time delays, we have analysed stability of the system for arbitrary values of the three time delays.

REFERENCES

Breda, D., Maset, S., and Vermiglio, R. (2006). Pseudospectral approximation of eigenvalues of derivative operators with non-local boundary conditions. *Applied numerical mathematics*, 56(3), 318–331.

Cooke, K.L. and Grossman, Z. (1982). Discrete delay, distributed delay and stability switches. *Journal of Mathematical Analysis and Applications*, 86(2), 592–627.

Dauer, W. and Przedborski, S. (2003). Parkinson's disease: mechanisms and models. *Neuron*, 39(6), 889–909.

Fujimoto, K. and Kita, H. (1993). Response characteristics of subthalamic neurons to the stimulation of the sensorimotor cortex in the rat. *Brain research*, 609(1), 185–192.

Gatev, P., Darbin, O., and Wichmann, T. (2006). Oscillations in the basal ganglia under normal conditions and in movement disorders. *Movement disorders*, 21(10), 1566–1577.

Götz, J., Schonrock, N., Vissel, B., and Ittner, L.M. (2009). Alzheimer's disease selective vulnerability and modeling in transgenic mice. *Journal of Alzheimer's Disease*, 18(2), 243–251.

Hallworth, N., Wilson, C., and Bevan, M. (2003). Apamin-sensitive small conductance calcium-activated potassium channels, through their selective coupling to voltage-gated calcium channels, are critical determinants of the precision, pace, and pattern of action potential generation in rat subthalamic nucleus neurons in vitro. *The Journal of neuroscience*, 23(20), 7525–7542.

Holgado, A.J.N., Terry, J.R., and Bogacz, R. (2010). Conditions for the generation of beta oscillations in the subthalamic nucleusglobus pallidus network. *The Journal of Neuroscience*, 30(37), 12340–12352.

Kita, H., Chang, H., and Kitai, S. (1983). Pallidal inputs to subthalamus: intracellular analysis. *Brain research*, 264(2), 255–265.

Kita, H. and Kitai, S. (1991). Intracellular study of rat globus pallidus neurons: membrane properties and responses to neostriatal, subthalamic and nigral stimulation. *Brain research*, 564(2), 296–305.

Kita, H., Nambu, A., Kaneda, K., Tachibana, Y., and Takada, M. (2004). Role of ionotropic glutamatergic and gabaergic inputs on the firing activity of neurons in the external pallidum in awake monkeys. *Journal of neurophysiology*, 92(5), 3069–3084.

Kita, H. (2007). Globus pallidus external segment. *Progress in brain research*, 160, 111–133.

Kita, H., Tachibana, Y., Nambu, A., and Chiken, S. (2005). Balance of monosynaptic excitatory and disynaptic inhibitory responses of the globus pallidus induced after stimulation of the subthalamic nucleus in the monkey. *The Journal of Neuroscience*, 25(38), 8611–8619.

Lebedev, M. and Wise, S. (2000). Oscillations in the premotor cortex: single-unit activity from awake, behaving monkeys. *Experimental brain research*, 130(2), 195–215.

Little, S. and Brown, P. (2014). The functional role of beta oscillations in parkinson's disease. *Parkinsonism & related disorders*, 20, S44–S48.

Loiseau, J.J., Michiels, W., Niculescu, S.I., and Sipahi, R. (2009). *Topics in time delay systems: analysis, algorithms and control*, volume 388. Springer.

Merrison-Hort, R., Yousif, N., Njap, F., Hofmann, U.G., Burylko, O., and Borisyuk, R. (2013). An interactive channel model of the basal ganglia: bifurcation analysis under healthy and parkinsonian conditions. *The Journal of Mathematical Neuroscience*, 3(1), 14.

Nakanishi, H., Kita, H., and Kitai, S. (1987). Intracellular study of rat substantia nigra pars reticulata neurons in an in vitro slice preparation: electrical membrane properties and response characteristics to subthalamic stimulation. *Brain research*, 437(1), 45–55.

Pavlides, A., John Hogan, S., and Bogacz, R. (2012). Improved conditions for the generation of beta oscillations in the subthalamic nucleus–globus pallidus network. *European Journal of Neuroscience*, 36(2), 2229–2239.

Sanz-Arigita, E.J., Schoonheim, M.M., Damoiseaux, J.S., Rombouts, S.A., Maris, E., Barkhof, F., Scheltens, P., and Stam, C.J. (2010). Loss of small-worldnetworks in alzheimer's disease: graph analysis of fmri resting-state functional connectivity. *PloS ONE*, 5(11), e13788.

Schultz, W. and Romo, R. (1988). Neuronal activity in the monkey striatum during the initiation of movements. *Experimental Brain Research*, 71(2), 431–436.

Smith, Y., Wichmann, T., Factor, S.A., and DeLong, M.R. (2011). Parkinson's disease therapeutics: new developments and challenges since the introduction of levodopa. *Neuropsychopharmacology*, 37(1), 213–246.

Supekar, K., Menon, V., Rubin, D., Musen, M., and Greicius, M.D. (2008). Network analysis of intrinsic functional brain connectivity in alzheimer's disease. *PLoS computational biology*, 4(6), e1000100.

Wilson, H.R. and Cowan, J.D. (1972). Excitatory and inhibitory interactions in localized populations of model neurons. *Biophysical journal*, 12(1), 1–24.

Yao, N., Shek-Kwan Chang, R., Cheung, C., Pang, S., Lau, K.K., Suckling, J., Rowe, J.B., Yu, K., Ka-Fung Mak, H., Chua, S.E., et al. (2014). The default mode network is disrupted in parkinson's disease with visual hallucinations. *Human brain mapping*, 35(11), 5658–5666.

Zhang, D., Liu, X., Chen, J., and Liu, B. (2014). Distinguishing patients with parkinson's disease subtypes from normal controls based on functional network regional efficiencies. *PloS ONE*, 9(12), e115131.